

LETTER

doi:10.1038/nature21040

Observation of the 1S–2S transition in trapped antihydrogen

M. Ahmadi, B. X. R. Alves, C. J. Baker, W. Bertsche, E. Butler, A. Capra, C. Carruth, C. L. Cesar, M. Charlton, S. Cohen, R. Collister, S. Eriksson, A. Evans, N. Evetts, J. Fajans, T. Friesen, M. C. Fujiwara, D. R. Gill, A. Gutierrez, J. S. Hangst, W. N. Hardy, M. E. Hayden, C. A. Isaac, A. Ishida, M. A. Johnson, S. A. Jones, S. Jonsell, L. Kurchaninov, N. Madsen, M. Mathers, D. Maxwell, J. T. K. McKenna, S. Menary, J. M. Michan, T. Momose, J. J. Munich, P. Nolan, K. Olchanski, A. Olin, P. Pusa, C. Ø. Rasmussen, F. Robicheaux, R. L. Sacramento, M. Sameed, E. Sarid, D. M. Silveira, S. Stracka, G. Stutter, C. So, T. D. Tharp, J. E. Thompson, R. I. Thompson, D. P. van der Werf & J. S. Wurtele

This is a PDF file of a peer-reviewed paper that has been accepted for publication. Although unedited, the content has been subjected to preliminary formatting. *Nature* is providing this early version of the typeset paper as a service to our customers. The text and figures will undergo copyediting and a proof review before the paper is published in its final form. Please note that during the production process errors may be discovered which could affect the content, and all legal disclaimers apply.

Cite this article as: Ahmadi, M. *et al.* Observation of the 1S–2S transition in trapped antihydrogen. *Nature* <http://dx.doi.org/10.1038/nature21040> (2016).

Received 29 November; accepted 7 December 2016.

Accelerated Article Preview Published online 19 December 2016.

Observation of the 1S–2S transition in trapped antihydrogen

M. Ahmadi¹, B. X. R. Alves², C. J. Baker³, W. Bertsche^{4,5}, E. Butler⁶, A. Capra⁷, C. Carruth⁸, C. L. Cesar⁹, M. Charlton³, S. Cohen¹⁰, R. Collister⁷, S. Eriksson³, A. Evans¹¹, N. Evetts¹², J. Fajans⁸, T. Friesen², M. C. Fujiwara⁷, D. R. Gill⁷, A. Gutierrez¹³, J. S. Hangst², W. N. Hardy¹², M. E. Hayden¹⁴, C. A. Isaac³, A. Ishida¹⁵, M. A. Johnson^{4,5}, S. A. Jones³, S. Jonsell¹⁶, L. Kurchaninov⁷, N. Madsen³, M. Mathers¹⁷, D. Maxwell³, J. T. K. McKenna⁷, S. Menary¹⁷, J. M. Michan^{7,18}, T. Momose¹², J. J. Munich¹⁴, P. Nolan¹, K. Olchanski⁷, A. Olin^{7,19}, P. Pusa¹, C. Ø. Rasmussen², F. Robicheaux²⁰, R. L. Sacramento⁹, M. Sameed³, E. Sarid²¹, D. M. Silveira⁹, S. Stracka²², G. Stutter², C. So¹¹, T. D. Tharp²³, J. E. Thompson¹⁷, R. I. Thompson¹¹, D. P. van der Werf^{3,24} & J. S. Wurtele⁸

The spectrum of the hydrogen atom has played a central part in fundamental physics in the past 200 years. Historical examples of its significance include the wavelength measurements of absorption lines in the solar spectrum by Fraunhofer, the identification of transition lines by Balmer, Lyman *et al.*, the empirical description of allowed wavelengths by Rydberg, the quantum model of Bohr, the capability of quantum electrodynamics to precisely predict transition frequencies, and modern measurements of the 1S–2S transition by Hänsch¹ to a precision of a few parts in 10¹⁵. Recently, we have achieved the technological advances to allow us to focus on antihydrogen—the antimatter equivalent of hydrogen^{2,3,4}. The Standard Model predicts that there should have been equal amounts of matter and antimatter in the primordial Universe after the Big Bang, but today's Universe is observed to consist almost entirely of ordinary matter. This motivates physicists to carefully study antimatter, to see if there is a small asymmetry in the laws of physics that govern the two types of matter. In particular, the CPT (charge conjugation, parity reversal, time reversal) Theorem, a cornerstone of the Standard Model, requires that hydrogen and antihydrogen have the same spectrum. Here we report the observation of the 1S–2S transition in magnetically trapped atoms of antihydrogen in the ALPHA-2 apparatus at CERN. We determine that the frequency of the transition, driven by two photons from a laser at 243 nm, is consistent with that expected for hydrogen in the same environment. This laser excitation of a quantum state of an atom of antimatter represents a highly precise measurement performed on an anti-atom. Our result is consistent with CPT invariance at a relative precision of $\sim 2 \times 10^{-10}$.

Experimental comparison of the spectra of hydrogen and antihydrogen was one of the main scientific motivations for the construction of CERN's Antiproton Decelerator⁵ (AD). Of obvious utility is the 1S–2S transition, due to the long lifetime ($\sim 1/8$ of a second) of the 2S state and the attendant narrow frequency width of the transition (a few Hz at 2.5×10^{15} Hz). A comparison of the hydrogen and antihydrogen frequencies for this transition is thus potentially an extremely sensitive test of CPT symmetry. The technological challenges to addressing antihydrogen with laser light are, however, extreme, as antihydrogen does not occur naturally and must be synthesised and judiciously protected

from interaction with atoms of normal matter – which will annihilate it. Working with only a few anti-atoms at a time represents a further challenge, when compared to spectroscopy on 10¹² atoms of trapped hydrogen⁶.

Low energy antihydrogen was first synthesised² by the ATHENA collaboration in 2002. This feat was later repeated by the ATRAP⁷, ALPHA⁸, and ASACUSA⁹ collaborations. In 2010 the ALPHA team succeeded in trapping antihydrogen³ in order to facilitate its study. We subsequently showed that anti-atoms could be held⁴ for up to 1000 s, and we have performed various measurements on antihydrogen in the context of tests of CPT symmetry^{10,11,12} or gravitational studies¹³.

The central portion of ALPHA-2, our second-generation trapping device for antihydrogen, is shown schematically in Figure 1. Antihydrogen is synthesised by mixing plasmas of antiprotons from the AD ($\sim 90,000$ particles) and positrons from a Surko-type accumulator^{14,15} (~ 1.6 million particles). The techniques employed in this experiment yield about 25,000 antihydrogen atoms per mixing attempt.

Antihydrogen atoms can be trapped in the multipolar, superconducting trap if they have a kinetic energy of less than about 0.5 K (in temperature units). The trap comprises a set of 'mirror coils' – short solenoids that generate the axial confinement well – and an octupole for transverse confinement. Trapped antihydrogen is detected by ramping down the currents in the magnetic trap over 1.5 s and detecting the annihilation of the antiproton when the released atoms hit the wall of the trap. We employ a three-layer silicon vertex detector¹⁶ to image the annihilation vertex position of each detected atom. Event topology is used to distinguish antiproton annihilations from cosmic rays, which continually trigger the detector at an average rate of $(10.02 \pm 0.04) \text{ s}^{-1}$.

The particle manipulations necessary to produce trappable antihydrogen atoms have been described elsewhere^{3,4,17}; we note only that recent innovations (Methods) in these techniques have provided a large improvement in the number of trapped anti-atoms available per trial, compared to our most recent publication¹². The antihydrogen production employed below involves a new technique in which we 'stack' anti-atoms resulting from two successive mixing cycles, originating from independent shots of antiprotons from the AD and accumulations of positrons. We have trapped on average ~ 14 anti-atoms per trial for this work, compared to 1.2 in previous work¹².

¹Department of Physics, University of Liverpool, Liverpool L69 7ZE, UK. ²Department of Physics and Astronomy, Aarhus University, DK-8000 Aarhus C, Denmark. ³Department of Physics, College of Science, Swansea University, Swansea SA2 8PP, UK. ⁴School of Physics and Astronomy, University of Manchester, Manchester M12 9PL, UK. ⁵Cockcroft Institute, Sci-Tech Daresbury, Warrington WA4 4AD, UK. ⁶Physics Department, CERN, CH-1211 Geneva 23, Switzerland. ⁷TRIUMF, 4004 Wesbrook Mall, Vancouver, British Columbia V6T 2A3, Canada. ⁸Department of Physics, University of California at Berkeley, Berkeley, California 94720-7300, USA. ⁹Instituto de Física, Universidade Federal do Rio de Janeiro, Rio de Janeiro 21941-972, Brazil. ¹⁰Department of Physics, Ben-Gurion University of the Negev, Beer-Sheva 84105, Israel. ¹¹Department of Physics and Astronomy, University of Calgary, Calgary, Alberta T2N 1N4, Canada. ¹²Department of Physics and Astronomy, University of British Columbia, Vancouver, British Columbia V6T 1Z1, Canada. ¹³Department of Medical Physics and Biomedical Engineering, University College London, London WC1E 6BT, UK. ¹⁴Department of Physics, Simon Fraser University, Burnaby, British Columbia V5A 1S6, Canada. ¹⁵Department of Physics, The University of Tokyo, 7-3-1 Hongo, Bunkyo, Tokyo 113-0033, Japan. ¹⁶Department of Physics, Stockholm University, SE-10691 Stockholm, Sweden. ¹⁷Department of Physics and Astronomy, York University, Toronto, Ontario M3J 1P3, Canada. ¹⁸École Polytechnique Fédérale de Lausanne (EPFL), Swiss Plasma Center (SPC), Lausanne CH-1015, Switzerland. ¹⁹Department of Physics and Astronomy, University of Victoria, Victoria, British Columbia V8P 5C2, Canada. ²⁰Department of Physics and Astronomy, Purdue University, West Lafayette, Indiana 47907, USA. ²¹Soreq NRC, Yavne 81800, Israel. ²²Università di Pisa and Sezione INFN di Pisa, Largo Pontecorvo 3, 56127 Pisa, Italy. ²³Physics Department, Marquette University, PO Box 1881, Milwaukee, Wisconsin 53201-1881, USA. ²⁴IRFU, CEA/Saclay, F-91191, Gif-sur-Yvette Cedex, France.

The trapped anti-atoms are confined to a cylindrical volume of 44 mm diameter and 280 mm length. Windows in the vacuum chamber allow the introduction of 243 nm laser light into this cryogenic, ultra-high vacuum (UHV) volume. Two counter-propagating photons can excite the 1S-2S transition at a frequency independent of the Doppler effect to first order. To have enough light intensity in each direction to excite the anti-atoms in a reasonable amount of time, ALPHA-2 includes a Fabry-Pérot power build-up cavity in the UHV system (Figure 1).

The laser system (Figure 2) features a Toptica TA-FHG pro laser generating about 150 mW of 243 nm radiation obtained by twice frequency doubling light from a tunable, 972 nm diode laser. The UV light is transported to the internal cavity, which is locked to the laser frequency using the Pound-Drever-Hall¹⁸ (PDH) technique. A photodiode monitors the transmitted light to determine the cavity power.

The laser is stabilised by locking to an ultra-low expansion (ULE) cavity (Menlo Systems). An acousto-optic modulator (AOM) is used to shift the laser frequency from the antihydrogen transitions to the nearest ULE cavity mode. A femtosecond frequency comb (Menlo Systems), referenced to a GPS-disciplined quartz oscillator (K+K Messtechnik), monitors and corrects the drift of the ULE cavity and relates the laser frequency to atomic time.

The hypothesis to be investigated here is that the 1S-2S transition in antihydrogen is at the same frequency as that of hydrogen. Since our antihydrogen is confined in a magnetic field, we rely on the known physics of the hydrogen atom to calculate the expected frequency and excitation rates of the transition in trapped antihydrogen.

Figure 3 shows hyperfine energy levels of the 1S and 2S states in a magnetic field. The low-field seeking ground state sublevels, 1S_c and 1S_b, survive in the magnetic minimum trap and can be excited to the corresponding 2S hyperfine state. The transition frequencies, f_{c-c} and f_{d-d} are different primarily because the hyperfine splitting of the 1S and 2S states are different.

To simulate the experiment, we propagate the trapped atoms in an accurate model of the magnetic trap. Note that the longitudinal magnetic field profile (Figure 1b) is ‘flattened’ using the central three mirror coils, in order to maximise the volume of resonance overlap with the laser. When the atom crosses the laser beam, we calculate the two-photon excitation probability, taking into account transit time broadening, AC Stark shift, and residual Zeeman effect. An atom in the 2S state can be ionised by a single additional photon from the 243 nm laser, or it can decay in one of two ways: 1) a two-photon decay, which returns the atom to the same hyperfine state in which it started or, 2) a one-photon decay via the 2P state, which can mix with the 2S state due to the motional electric field the atoms experience in the magnetic trap. The single photon decays can result in trappable ground state atoms, or they can induce a spin-flip of the positron, resulting in a non-trappable atom that escapes and annihilates.

In Figure 4 we show the response of the simulated atoms to a 300 s exposure of both the c-c and d-d transitions, as a function of laser detuning, assuming 1 W of circulating laser power in the build-up cavity. The response is asymmetric with a tail at higher frequencies due to the residual Zeeman effect. In the inset of Figure 4, we show the population in the different end states after illuminating each of the transitions for a time t with zero laser detuning. The fraction of anti-atoms removed by the on-resonance laser, compared to off resonance, is estimated to be 0.47 at 300 s.

The experimental protocol is very straightforward and has been previously applied to our demonstration of microwave-induced transitions¹⁰ in trapped antihydrogen. A single experimental trial involves producing antihydrogen in the atom trap, pulsing axial electric fields to rid the trap of residual charged particles, holding the trapped anti-atoms for 600 s, and then ramping down the trapping fields to release and detect any anti-atoms in the trap.

Three types of trials were conducted. 1) ‘On resonance’: After the antihydrogen has been produced, trapped and allowed to decay to the

ground state, the laser is tuned to an expected resonance frequency for one of the 1S-2S transitions, introduced into the trapping volume, and the internal cavity is locked. The d-d transition and then the c-c transition are driven for 300 s each. 2) ‘Off resonance’: Same as above but the laser is detuned 200 kHz (at 243 nm) below the relevant transition. 3) ‘No laser’: No laser radiation is present during the 600 s hold time. During the hold times, electrostatic blocking potentials are placed on electrodes to either side of the magnetic trap (Figure 1) to ensure that antiprotons resulting from ionisation can only be lost radially. Electric fields from these potentials are negligible in the anti-atom trapping volume.

In all aspects other than the laser configuration, the three trial sequences are identical. The on-resonance laser frequencies employed correspond to transition frequencies (twice the laser frequency) of:

$$f_{d-d} = 2\,466\,061\,103\,064\ (2)\ \text{kHz}$$

$$f_{c-c} = 2\,466\,061\,707\,104\ (2)\ \text{kHz}$$

There is no measurable laser power difference between these and their respective off-resonance counterparts.

We have conducted 11 sets of the three types of trial, varying the order within each set to reduce the chance of systematic effects. Alternating the trials in this fashion ameliorates the effects of a slow decline in the trapping rate over the course of the experiment.

We use a multivariate analysis (MVA, Methods) algorithm¹⁰ to distinguish antiproton annihilations from cosmic rays. The MVA used for the 1.5 s shutdown window yields a cosmic ray background rate of $(0.042 \pm 0.001)\ \text{s}^{-1}$, or 0.062 events per trial. This is the only significant detector background in the experiment. The event reconstruction efficiency (ratio of the number of events identified as antiproton annihilations to the number of detector triggers) is 0.688 ± 0.002 (Methods).

The results of the experiment, summed over 11 trials, are shown in Table 1, and show a very significant difference between the on and off resonance trials (C-test¹⁹, one-sided p-value of 4.2×10^{-10}).

We use the ‘no laser’ trials to ensure that any fluctuation in the trapping rate is small compared to the difference between subsequent on resonance and off resonance trials. The comparison of off resonance and no laser rates confirms that there are no laser-related side effects (e.g. vacuum degradation) that lead to antihydrogen loss from the trap.

The on and off resonance trials differ by 92 ± 15 counts. We conclude that the laser light has removed $(58 \pm 6)\%$ of the trapped antihydrogen atoms by resonant 1S-2S excitation followed by either a spin flip or an ionisation event. The removed fraction is in good agreement with the hydrogenic rate estimates in Figure 4, for our build-up cavity power of 1 W.

Our sensitive vertex detector allows us to search for evidence of annihilations during the 2 x 300 s hold periods. Due to the long exposure times, we use a different MVA protocol (Methods) to distinguish events from background. With this protocol, the cosmic background rate is reduced to $0.0043 \pm 0.0003\ \text{s}^{-1}$ at the expense of reducing the reconstruction efficiency to 0.376 ± 0.002 . A summary of this analysis for the same 11 sets of trials is shown in Table 2.

Here, the summed off-resonance and no laser trials are generally consistent with background only, and the difference between the on and off resonance totals of 52 ± 10 counts shows clear statistical significance (C-test¹⁹, one-sided p-value of 2.2×10^{-7}). If the relative efficiencies are taken into account, the number of annihilations here ($52/0.376 \cong 138$) is in good agreement with the expected number of antihydrogen lost ($92/0.688 \cong 134$) from Table 1. These events may be due to either spin-flip of antihydrogen or radial loss of antiprotons resulting from ionisation.

If we assume that there are no exotic asymmetries in the spectrum of antihydrogen (compared to that of hydrogen) the 400 kHz resolution of the current observation, coupled with our model spectrum, can be interpreted as a test of CPT symmetry at a precision of 200 ppt.

A stronger statement of CPT invariance must await a detailed measurement of the transition line shape. For smaller detunings, the laser frequency determination, the laser linewidth and the uncertainty in determining the minimum magnetic field in the trap can become important. The long-term average laser frequency at 972 nm is determined to a relative accuracy of 8×10^{-13} using the frequency comb. The laser linewidth contributes at most 10 kHz to the uncertainty at the two-photon frequency, based on the measured excursions of the ULE cavity lock and worst-case fluctuations in the doubling stages. The uncertainty in the trap's minimum magnetic field strength is determined from the measured electron cyclotron frequency²⁰ of (28.46 ± 0.01) GHz. The field uncertainty leads to a frequency uncertainty of ± 6400 Hz and ± 350 Hz for the c-c and d-d transitions respectively (5.2×10^{-12} and 2.8×10^{-13} relative to the transition frequencies). Thus a straightforward extension of the current technique should provide a measurement of the lineshape in the near future.

We have performed the first laser-spectroscopic measurement on an atom of antimatter. This has long been a sought-after achievement in low-energy antimatter physics. It marks a turning point from proof-of-principle experiments to serious metrology and precision CPT comparisons using the optical spectrum of an anti-atom. The greatly improved trapping rate demonstrated here bodes well for many other future antihydrogen experiments, including microwave hyperfine transitions, spectroscopy and laser cooling using Lyman-alpha light²¹ and gravitational studies with neutral antimatter. The current result, along with recent limits on the antiproton-electron mass ratio²² by the ASACUSA collaboration and antiproton charge-to-mass ratio²³ by the BASE collaboration, demonstrate that tests of fundamental symmetries with antimatter at the AD are maturing rapidly.

We note in passing that the sensitivity of this initial measurement, in terms of the absolute energy scale, is $\sim 2 \times 10^{-18}$ GeV, which is approaching the absolute precision of the CPT test in the neutral kaon system of $\sim 5 \times 10^{-19}$ GeV²⁴. We also note that our antihydrogen measurements can potentially have a significant sensitivity to the internal structure of the antiproton, at a level relevant to the current puzzle in the proton charge radius^{25,26}.

Online Content Methods, along with any additional Extended Data display items and Source Data, are available in the online version of the paper; references unique to these sections appear only in the online paper.

Received 29 November; accepted 7 December 2016.

Published online 19 December 2016.

1. Parthey, C. G. *et al.* Improved measurement of the hydrogen 1S-2S transition frequency. *Phys. Rev. Lett.* **107**, 203001 (2011).
2. Amoretti, M. *et al.* Production and detection of cold antihydrogen atoms. *Nature* **419**, 456–459 (2002).
3. Andresen, G. B. *et al.* Trapped antihydrogen. *Nature* **468**, 673–676 (2010).
4. Andresen, G. B. *et al.* Confinement of antihydrogen for 1,000 seconds. *Nature Phys.* **7**, 558–564 (2011).
5. Maury, S. The antiproton decelerator: AD. *Hyp. Int.* **109**, 43–52 (1997).
6. Cesar, C. L. *et al.* Two-photon spectroscopy of trapped atomic hydrogen. *Phys. Rev. Lett.* **77**, 255–258 (1996).
7. Gabrielse, G. *et al.* Background-free observation of cold antihydrogen with field-ionization analysis of its states. *Phys. Rev. Lett.* **89**, 213401 (2002).
8. Andresen, G. B. *et al.* Production of antihydrogen at reduced magnetic field for anti-atom trapping. *J. Phys. B* **41**, 011001 (2008).
9. Enomoto, Y. *et al.* Synthesis of cold antihydrogen in a cusp trap. *Phys. Rev. Lett.* **105**, 243401 (2010).
10. Amole, C. *et al.* Resonant quantum transitions in trapped antihydrogen atoms. *Nature* **483**, 439–443 (2012).
11. Amole, C. *et al.* Experimental limit on the charge of antihydrogen. *Nature Commun.* **5**, 3955 (2014).
12. Ahmadi, M. *et al.* An improved limit on the charge of antihydrogen from stochastic acceleration. *Nature* **529**, 373–376 (2016).


13. Amole, C. *et al.* Description and first application of a new technique to measure the gravitational mass of antihydrogen. *Nature Commun.* **4**, 1785 (2013).
14. Murphy, T. & Surko, C. Positron trapping in an electrostatic well by inelastic collisions with nitrogen molecules. *Phys. Rev. A* **46**, 5696–5705 (1992).
15. Surko, C. M., Greaves, R. G. & Charlton, M. Stored positrons for antihydrogen production. *Hyp. Int.* **109**, 181–188 (1997).
16. Amole, C. *et al.* Silicon vertex detector upgrade in the ALPHA experiment. *Nucl. Instrum. Methods Phys. Res. A* **732**, 134–136 (2013).
17. Andresen, G. B. *et al.* Search for trapped antihydrogen. *Phys. Lett. B* **695**, 95–104 (2011).
18. Drever, R. W. P., Hall, J. L., Kowalski, F. V., Hough, J., Ford, G. M., Munley, A. J., & Ward, H. Laser phase and frequency stabilization using an optical resonator. *Applied Physics B: Lasers and Optics* **31**, pp. 97–105 (1983).
19. Przyborowski, J. & Wilenski, H. Homogeneity of results in testing samples from Poisson series. *Biometrika* **31**, 313–323 (1940).
20. Amole, C. *et al.* In situ electromagnetic field diagnostics with an electron plasma in a Penning-Malmberg trap. *New J. Phys.* **16**, 013037 (2014).
21. Donnan, P. H., Fujiwara, M. C. & Robicheaux, F. A proposal for laser cooling antihydrogen atoms. *J. Phys. B* **46**, 025302 (2013).
22. Hori, M., *et al.* Buffer-gas cooling of antiprotonic helium to 1.5 to 1.7 K, and antiproton-to-electron mass ratio. *Science* **354**, 610–614 (2016).
23. Ulmer, S. *et al.* High precision comparison of the antiproton-to-proton charge-to-mass ratio. *Nature* **524**, 196–199 (2015).
24. Particle Data Group (J. Beringer *et al.*) 1528 pp., Published in *Phys. Rev. D* **86** 010001 (2012).
25. Pohl, R. *et al.* The size of the proton. *Nature* **466**, 213–216 (2010).
26. Pohl, R. *et al.* Laser spectroscopy of muonic deuterium. *Science* **353**, 669–673 (2016).

Acknowledgements All authors are members of the ALPHA Collaboration.

This work was supported by: the European Research Council through its Advanced Grant programme (JSH); CNPq, FAPERJ, RENAFEA (Brazil); NSERC, NRC/TRIUMF, EHPDS/EHDRS, FORNT (Canada); FNU (Nice Centre), Carlsberg Foundation (Denmark); JSPS Postdoctoral Fellowships for Research Abroad (Japan); ISF (Israel); STFC, EPSRC, the Royal Society and the Leverhulme Trust (UK); DOE, NSF (USA); and VR (Sweden). We are grateful for the efforts of the CERN AD team, without which these experiments could not have taken place. We thank Jacky Tonoli (CERN) and his staff for extensive, time-critical help with machining work. We thank the staff of the Superconducting Magnet Division at Brookhaven National Laboratory for collaboration and fabrication of the trapping magnets. We thank C. Marshall (TRIUMF) for his work on the ALPHA-2 cryostat. We acknowledge the profound influence of Professor T. Hänsch on the methodology and the hardware employed here. We thank Professor F. Besenbacher (Aarhus) for timely support in procuring the ALPHA-2 external solenoid. We thank A. Charman (UC Berkeley) for many useful discussions.

Author Contributions This experiment was based on data collected using the ALPHA-2 antihydrogen trapping apparatus, designed and constructed by the ALPHA Collaboration using methods developed by the entire collaboration. The entire collaboration participated in the operation of the apparatus and the data taking activities. The laser and internal cavity system was conceived, implemented, commissioned and operated by WB, NM, JSH, SE, CØR, SAJ, CLC, BXRA and GS. FR, CØR, JF and NM developed the simulation program for laser interaction with magnetically trapped atoms. New techniques for obtaining a higher antihydrogen trapping rate and realising antihydrogen stacking were proposed and implemented by CC, WB, JF, TF, SAJ, NM, DM, CØR, CB and MS. Detailed analysis of the antiproton annihilation detector data was done by JTKM and AO, using methods introduced to ALPHA by SS. The positron accumulator is the responsibility of CB, MC, CAI and DPW. The manuscript was written by JSH, SE, SAJ, NM, CØR, and JTKM, with extensive help from CLC, MCF, JF, AO and MEH. The manuscript was then edited and improved by the entire collaboration. Much of the work in this article forms part of the PhD theses of CØR and SAJ.

Author Information Reprints and permissions information is available at www.nature.com/reprints. The authors declare no competing financial interests. Readers are welcome to comment on the online version of the paper. Correspondence and requests for materials should be addressed to JSH (jeffrey.hangst@cern.ch).

 This work is licensed under a Creative Commons Attribution 4.0 International (CC BY 4.0) licence. The images or other third party material in this article are included in the article's Creative Commons licence, unless indicated otherwise in the credit line; if the material is not included under the Creative Commons licence, users will need to obtain permission from the licence holder to reproduce the material. To view a copy of this licence, visit <http://creativecommons.org/licenses/by/4.0/>

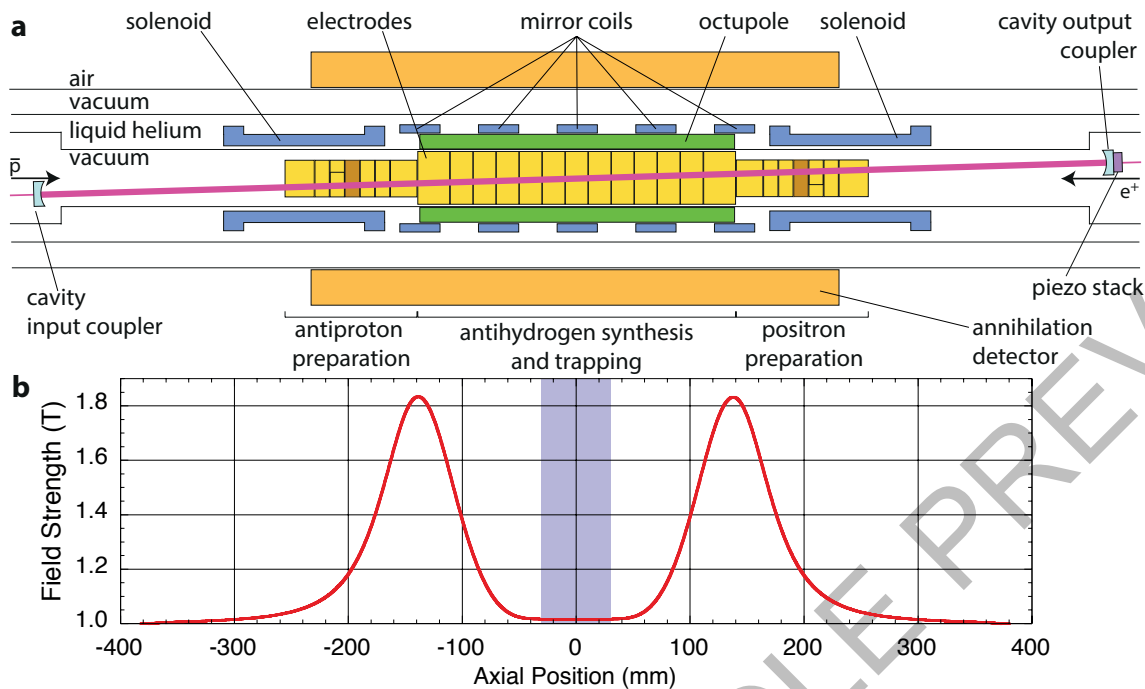


Figure 1 | The ALPHA-2 central apparatus and magnetic field profile.

a. The various Penning traps (electrodes + 1 T external solenoid, not shown) confine and manipulate antiprotons and positrons to produce antihydrogen. Cold (< 0.5 K) anti-atoms are confined radially by the octupole field and axially by the magnetic well formed by the five mirror coils and plotted in **b**. Earlier experiments in ALPHA used only the end mirror coils. The flattened profile here (uniform to $\pm 10^{-4}$ T on axis in the shaded region) extends the laser resonance volume and slightly improves

the depth of the trap. Laser light enters from the antiproton side (left in the figure) and is aligned with the fixed cavity axis. The laser beam crosses the trap axis at an angle of 2.3° . The piezoelectric actuator on the output coupler is used to lock the cavity to the laser frequency. The two figures **a** and **b** have the same axial scale; the radial extent of the annihilation detector is larger than illustrated. The brown-shaded electrodes are used to apply blocking potentials during the experimental trials (see text).

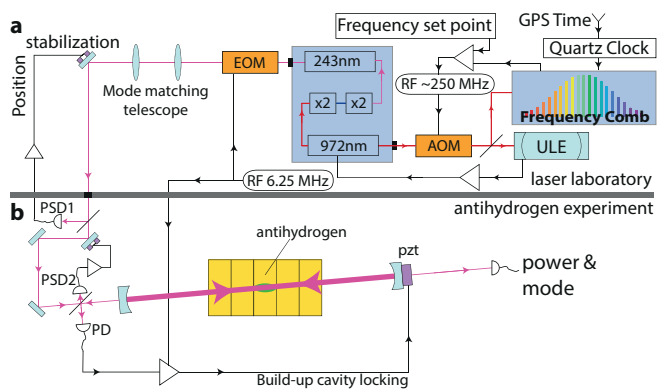


Figure 2 | Schematic of the laser setup. **a.** Light from the 243 nm laser passes through an electro-optic modulator (EOM) for 6.25 MHz sideband creation, and a Galilean telescope to mode-match the beam to the build-up cavity inside ALPHA-2. The 243 nm light is generated by frequency quadrupling the output of a 972 nm diode laser. The 972 nm light is shifted to resonance with an ultra low expansion glass Fabry-Perot cavity (ULE) by an acousto-optic modulator (AOM), which also serves to stabilise the laser frequency. The ULE frequency is referenced to the SI second by an optical frequency comb, stabilised by a GPS-disciplined quartz oscillator. The ULE resonance together with the chosen frequency set point determines the AOM modulation frequency. **b.** The 243 nm laser beam is transported through air to the ALPHA-2 apparatus. Beam position and angle are stabilised through an active feedback system using position sensitive detectors (PSD) and piezo-actuated mirrors. The reflection from the input coupler of the build-up cavity is picked up with a photo diode (PD) and mixed with the sideband frequency to provide the Pound-Drever-Hall locking signal for the piezo-mounted output coupler. The transmitted light is continuously monitored both with a PD for power measurement and a CCD camera for mode monitoring. The build-up cavity has a finesse of 230, providing a circulating power greater than 1 W once losses are taken into account.

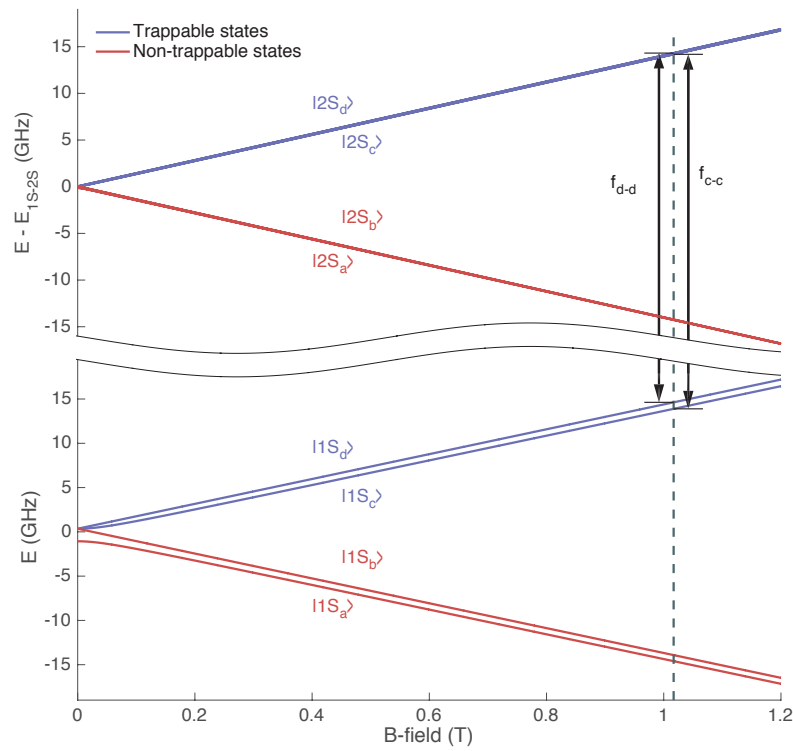


Figure 3 | Hydrogenic energy levels. Calculated energies (for hydrogen) of the hyperfine sublevels of the 1S and 2S states as functions of magnetic field strength. To show the structure of the sublevels, the centroid energy difference, $E_{1S-2S} = 2.4661 \times 10^{15}$ Hz, has been suppressed on the vertical axis. Vertical black arrows indicate the two-photon transitions between the trappable 1S and 2S states.

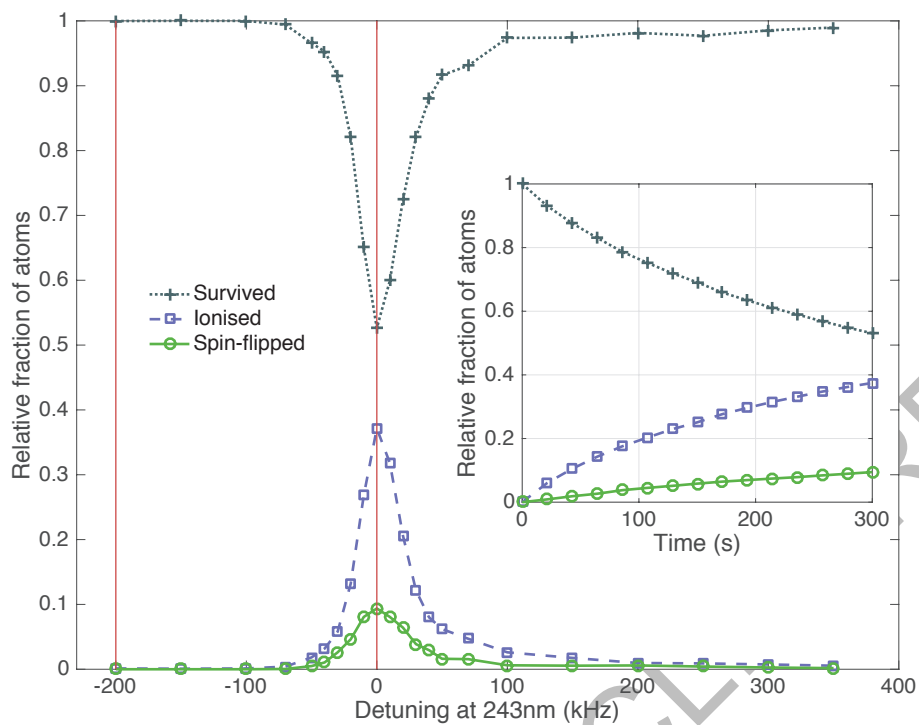


Figure 4 | Simulation results. Simulated results of illuminating both the c-c and d-d transitions for 300 s with 1W of circulating laser power. Survival or removal fraction is plotted as a function of laser detuning, where zero detuning is resonant at the field minimum of the magnetic trap. The vertical red lines indicate the detuning for off resonance

and on resonance illumination transitions in the experiment. **Inset.** Time evolution of populations in the relevant end states in the case of zero detuning. The populations are normalized to the simulated null experiment, *i.e.*, the number of atoms after an equal hold time with no laser interaction.

Table 1 | Detected events during the 1.5 s ramp down of the trap magnets

Type	Number of detected events	Background	Uncertainty
Off resonance	159	0.7	13
On resonance	67	0.7	8.2
No laser	142	0.7	12

ACCELERATED ARTICLE PREVIEW

Table 2 | Detected events during the 300 s hold times for each transition, and their sum

Type	Number of detected events	Expected Background	Uncertainty
d-d off res.	15	14.2	3.9
d-d on res.	39	14.2	6.2
No laser	22	14.2	4.7
c-c off res.	12	14.2	3.5
c-c on res.	40	14.2	6.3
No laser	8	14.2	2.8
d-d + c-c off res.	27	28.4	5.2
d-d + c-c on res.	79	28.4	8.9
No laser (sum)	30	28.4	5.5

ACCELERATED ARTICLE PREVIEW

METHODS

Time Evolution of the Dataset. The time evolution of the detected events in the three types of trials is depicted in Extended Data Figure 1.

Suppression of Cosmic Ray Background. To determine the signal events in the a) 1.5 s and b) 2 x 300 s observation windows, we require two different suppression techniques. We tune the MVA for the two windows in a similar manner to that used in our recent study of the neutrality of antihydrogen¹². Annihilation events are distinguished from background events (primarily cosmic rays) by their distinctive topologies. Nine selection variables sensitive to the difference between annihilation and background¹⁰ have been used as input to a multivariate analysis package^{27,28}.

The signal data and background data used for MVA training, validation and testing is a set of 207535 annihilation events and 1596579 background events. The signal events were produced during antiproton/positron mixing in the apparatus, and contain less than 1% background. Background events were collected during times when there was no antiproton beam.

a. The 1.5 s observation window. The analysis was tuned to give the same background rate (0.042 s^{-1}) as our 'online' analysis. This gave an efficiency of 0.688 ± 0.002 (statistical error only) annihilations/detector trigger.

b. The 300 s observation windows. The experimental data were accumulated over the 600 s/trial irradiation time, so a more severe suppression of the background was required. This MVA was optimized to give the best significance for the estimated number of annihilation events expected, suppressing the background rate to $0.0043 \pm 0.0003 \text{ s}^{-1}$, or an expected (2.57 ± 0.08) per 600 s trial. The corresponding efficiency is 0.376 ± 0.002 (statistical error only), or 54% of the value for the 1.5 s window.

Improved antihydrogen trapping rate. The improved trapping rate reported here is not the result of any single new technique or manipulation, but is rather due to very careful preparation and control of the charged species (electrons, antiprotons and positrons) used in the process of synthesising antihydrogen. At every step in the process, the particle plasmas are optimized for temperature, density, number and radial extent. ALPHA-2 is equipped with extensive diagnostics for lepton and antiproton plasmas. Potential manipulations are carefully controlled to create and maintain temperatures as low as possible for the positrons and antiprotons during mixing. We use such techniques as strong drive rotating wall electric fields²⁹ for controlling plasma sizes, and evaporative cooling³⁰ for obtaining low temperatures.

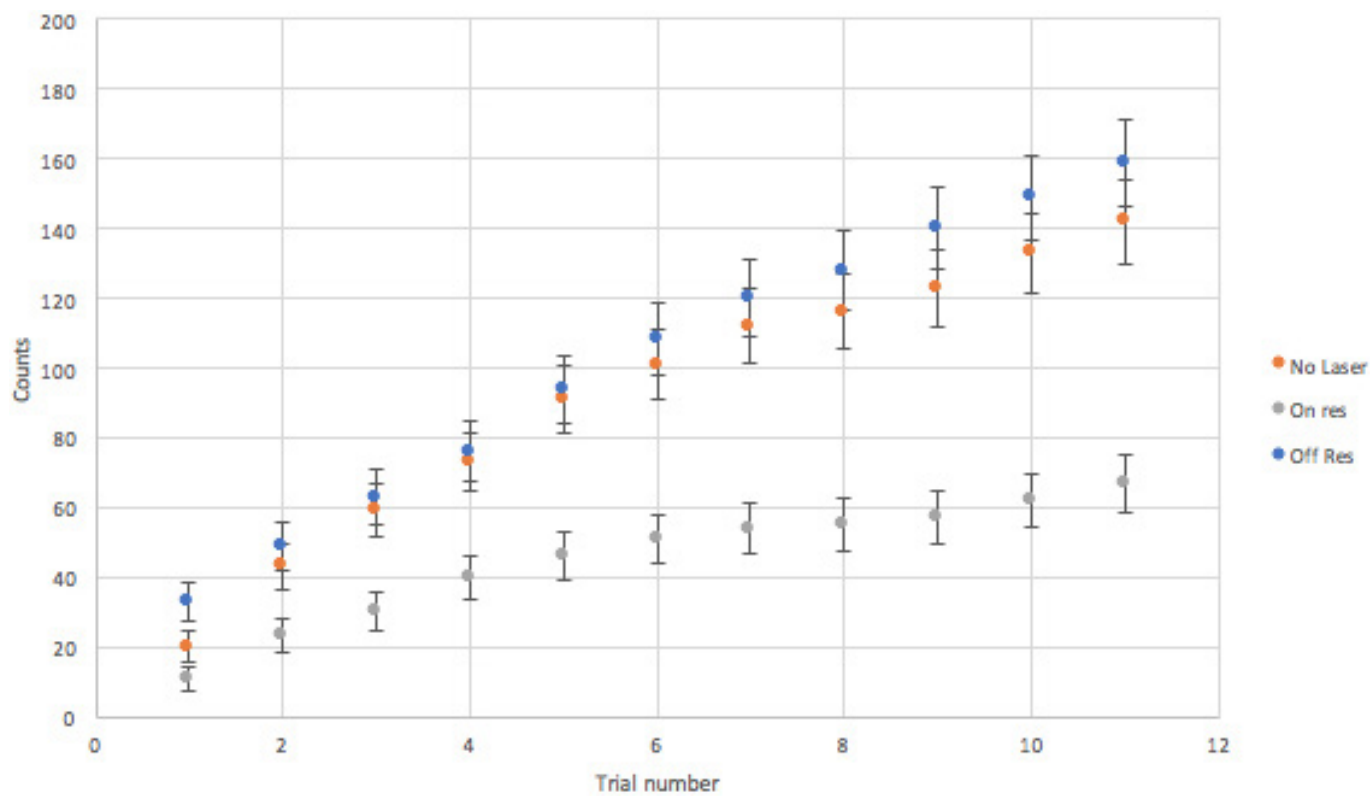
In order to maintain the lowest possible temperatures during mixing we synthesise antihydrogen by potential manipulation³¹ rather than the autoresonant drive technique³² used in more recent work. Our position-sensitive vertex detector is essential in analysing and optimising the mixing process, giving rapid feedback on the antihydrogen production rate, the time evolution of the rate, and the spatial distribution of the produced anti-atoms³¹.

The stacking technique for accumulating two loads of antihydrogen in the atom trap relies on the same careful preparation techniques in order to load a second batch of charged particles (antiprotons and positrons) into the trapping volume after the trapping fields have been energized and antihydrogen produced. In all previous publications^{3,4,10,11,12}, we have prepared the plasmas before ramping up the trapping fields.

In a departure from our previous work³, we do not use an extremely rapid (9 ms time constant) shutdown of the trapping fields to release trapped antihydrogen at the end of a trial. The fields are ramped down over 1.5 s instead. This leads to a higher overall duty cycle, as the rapid shutdown heats the Penning trap electrodes and quenches the superconducting magnets, requiring a wait of several minutes between trials to re-cool the apparatus to optimal cryogenic temperatures.

Data availability. The datasets generated during and/or analysed during the current study are available from the corresponding author (jeffrey.hangst@cern.ch) on reasonable request.

27. Narsky, I. StatPatternRecognition: a C++ package for statistical analysis of high energy physics data. Preprint at <http://arxiv.org/abs/physics/0507143> (2005).
28. Narsky, I. Optimization of signal significance by bagging decision trees. Preprint at <http://arxiv.org/abs/physics/0507157> (2005).
29. Danielson, J.R. & Surko, C. M. Radial compression and torque-balanced steady states of single-component plasmas in Penning-Malmberg traps, *Physics of Plasmas* **13**, 055706 (2006).
30. Andresen, G.B., *et al.* Evaporative cooling of antiprotons to cryogenic temperatures. *Phys. Rev. Lett.* **105**, 013003 (2010).
31. Andresen, G.B., *et al.* Antihydrogen formation dynamics in a multipolar neutral anti-atom trap. *Phys. Lett. B* **685**, 141 (2010).
32. Andresen, G. B. *et al.* Autoresonant excitation of antiproton plasmas. *Phys. Rev. Lett.* **106**, 025002 (2011).



Extended Data Figure 1 | Time evolution of the dataset. The cumulative number of observed events for each type of trial (On-res = on-resonance; off-res = off resonance) is plotted as a function of chronological trial number to illustrate the time history of the dataset. The errors are due to counting statistics ($\text{Sqrt}(N)$) only.